

# Crystallization of some anorthite–diopside glass precursors

C. LEONELLI, T. MANFREDINI, M. PAGANELLI, P. POZZI, G. C. PELLACANI  
*Dipartimento di Chimica, Università di Modena, Via Campi 183, 41100 Modena, Italy*

Anorthite and diopside have been obtained from complete devitrification of glasses belonging to the quaternary system  $\text{MgO-CaO-Al}_2\text{O}_3\text{-SiO}_2$ . Microstructure, the natural trend of the nucleation mechanism and kinetic studies on the crystallization phenomenon have been investigated by means of optical and electron microscopies, thermal and thermomechanical techniques and X-ray powder diffractometry. All the glasses investigated show a complete crystallization starting from a simple surface nucleation process. The activation energy for the crystallization process proved to be higher than that for viscous flow, leading to an important aspect modification in the sample during ceramization. Thermal stability and physical properties of both glass and glass–ceramic materials have been tested, suggesting the possible use of these materials in industrial application.

## 1. Introduction

Glass–ceramics are microcrystalline materials obtained from a parent glass by almost complete devitrification. Controlled crystallization of glass, starting from a heterogeneous or homogeneous nucleation process, can occur in two different ways depending on the nature of the nucleation mechanism. If nucleation occurs at a phase boundary between the vessel surface or air and the glass, the crystallization proceeds from the glass surface into the bulk material (surface crystallization).

The other type of nucleation (internal crystallization) can usually be achieved with a simple two-step heat-treatment; the first step is an isotherm at a temperature at which the mobility of atoms in the glass is sufficient for embryo formation and then nucleus growth. The second step is necessary to enhance crystal growth up to the desired size homogeneously dispersed in the volume [1].

Surface crystallization is favoured more than internal crystal nucleation, which generally necessitates the addition of nucleating agents. In fact if the first step of internal nucleation is ignored, only the surface and impurities inside the glass act as nuclei and the crystalline phase starts to grow on them.

Independent of nucleation mechanism, during crystal growth all mobile ions can move into the crystals leaving the glassy phase more and more viscous. This is the case for many glass–ceramic systems where the materials are partially devitrified in some preferential areas, leading to a dangerous anisotropy in chemical and physical properties [2–4].

Among glass–ceramic systems the quaternary  $\text{MgO-CaO-Al}_2\text{O}_3\text{-SiO}_2$  has been generally studied by considering the effect of the added oxides on the nucleation and crystallization mechanisms [1, 5–9]. In this paper we investigated the natural trend of the  $\text{MgO-CaO-Al}_2\text{O}_3\text{-SiO}_2$  system towards nucleation

in the absence of nucleating agents [10] with the aim of identifying the nucleation mechanism, along with the determination of the crystal growth activation energy. Further interest derives from the standpoint that, since the phenomenon of great difference between the physico-chemical properties of the newly formed crystals and the remaining vitreous phase is very common, it seems very important, also for possible industrial applications, to plan the devitrification of particular types of crystal which will have physical and chemical characteristics similar to those of the starting glassy phase.

## 2. Experimental procedure

### 2.1. Glass preparation

The compositions studied are listed in Table I. They were prepared from high-quality oxides and carbonates, melted in mullite crucibles using an electric furnace and quenched either in water or on an iron mould to obtain respectively frits and bars suitable for thermomechanical testing. The fusion temperature was about 1370 °C and in some cases a remelting of frits to assure homogeneity in the specimen was necessary. It has to be noted that the composition A75-D25 was not poured out of the crucible because of its partial devitrification and consequently exceptionally high viscosity. The chemical composition was checked to be constant even after the quenching process. No annealing treatment was performed either on the frits or on the bars.

### 2.2. Crystallization process

A quick heat treatment was used to prepare glass–ceramic samples: after heating at about 500 °C h<sup>-1</sup> an isotherm step at 1100 °C was held for 1 h, and then the

TABLE I Molar compositions (%) of the glasses studied

Composition	Content (mol %)			
	SiO <sub>2</sub>	Al <sub>2</sub> O <sub>3</sub>	CaO	MgO
A25-D75	50.10	5.15	25.03	19.72
A50-D50	50.07	10.93	25.03	13.97
A75-D25	50.04	17.49	25.03	7.44

specimens were extracted hot from the furnace and naturally cooled down to room temperature.

The crystal growth was followed by differential thermal analysis (DTA) in a Netzsch STA 409 thermobalance. Ground glassy frits with different grain sizes were heated at about 1400 °C at different heating rates and DTA data were collected also during controlled cooling to 300 °C. Tests on bulk glass were performed using specimens in the form of the DTA platinum crucible.

Thermomechanical measurements were performed in a Netzsch dilatometer and collected both on glass bars and on glass-ceramic bars with a heating rate of 10 °C min<sup>-1</sup>.

### 2.3. Microstructural analysis

The majority of microstructure studies on the crystallized glass were done by optical microscopy and by scanning electron microscopy (Philips PSEM 500). Sample preparation did not require any replica methods since freshly fractured or superficially etched specimens were suitable for this study.

Crystalline phases on glass-ceramic bar specimens, ground in an agate mill with agate balls for 20 min and sieved at 20 µm, were identified by X-ray powder diffractometry with nickel-filtered CuK<sub>α</sub> (λ = 0.15418 nm, Philips PW 1050) with a 2 s time constant and 1000 counts range in the 2θ range from 10 to 45° at a scanning rate of 1° min<sup>-1</sup>.

## 3. Results and discussion

### 3.1. Thermal and thermomechanical results

The compositions investigated belong to the region of glass formation in the ternary phase diagrams (Fig. 1) where pyroxenes (e.g. diopside) or anorthite are more stable [11]. The ease with which crystals are obtained from the melt of composition A75-D25 (Fig. 2), even during the quenching operations, impedes the formation of a pure glassy sample. Only A25-D75 and A50-D50 compositions transformed into glasses which were optically clear, bubble-free and homogeneous to polarized light.

The complete DTA thermograms of the three glass formulations investigated are shown in Fig. 3. Some very similar features of each thermogram are apparent:

(a) A reversible endothermic peak due to an increase of specific heat is present in the 720–740 °C temperature range, signifying the glass transition ( $T_G$ ). The

peak maxima move slightly toward higher temperatures with increasing amount of anorthite in the samples.

(b) There is an exothermic event indicating crystallization ( $T_C$ ) with a maximum at about 970–1000 °C for all the glasses, which shifts by only 25 °C to lower temperatures by increasing the anorthite content. A smaller peak area for composition A75-D25 confirms the presence of already crystallized material, which was absent in the other samples.

(c) An additional endothermic event, occurring at 1250–1300 °C, involves the melting of the glassy phases present. In particular, for the composition A25-D75 a double melting peak is observed at 1300 and 1280 °C: the first corresponds to the melting point of pure diopside, which is the main crystalline phase present, while the second can be correlated to that of the remaining glassy phase.

(d) During cooling an exothermic peak, well resolved from the melting point, is only observed for the A25-D75 and A50-D50 systems. This may indicate a crystallization process occurring during slow cooling, even though the drastic change in the physical state of the specimen can involve problems of interpretation. It is reasonable to assume, for these two compositions, that there exists a region of metastable non-crystalline state in a temperature range between the melting and crystallization temperatures. For the A75-D25 system, the presence of the lowest crystallization peak during heating and its absence during cooling indicates the initial existence of a crystalline phase which completes its formation during heating and does not melt at 1300 °C to form an amorphous phase which could recrystallize during cooling at 900 °C. This can be a direct indication that this composition gives rise to an unstable amorphous state, explainable as an anorthite and glass solid solution.

An important observation can be made on considering that the exothermic crystallization peak does not double even in the case of composition A50-D50, where the formation of both anorthite and diopside is verified to occur simultaneously. This can be an indirect evaluation of the small difference between the activation energies of formation for the two crystals.

In order to evaluate the nucleation mechanisms of the A50-D50 and A25-D75 glasses, samples with different specific surface areas were studied by DTA. The increase of the specific surface area does not significantly influence the glass transition temperatures, whereas the crystallization peak maxima relevantly shift toward lower temperatures (Table II and Fig. 4). This observation and the absence of the splitting of the exothermic peak strongly suggest that the mechanism of crystal growth is essentially determined by the surface nucleation [1, 12]. It is also noted that the transition temperatures of these glasses are located in a very narrow temperature range (720–730 °C) which does not move even while changing heating rate or particle size. This suggests that glasses from these compositions are quite stable up to the glass transformation temperature.

Thermomechanical behaviour of the parent glass and the crystallized material are very similar (Fig. 5),

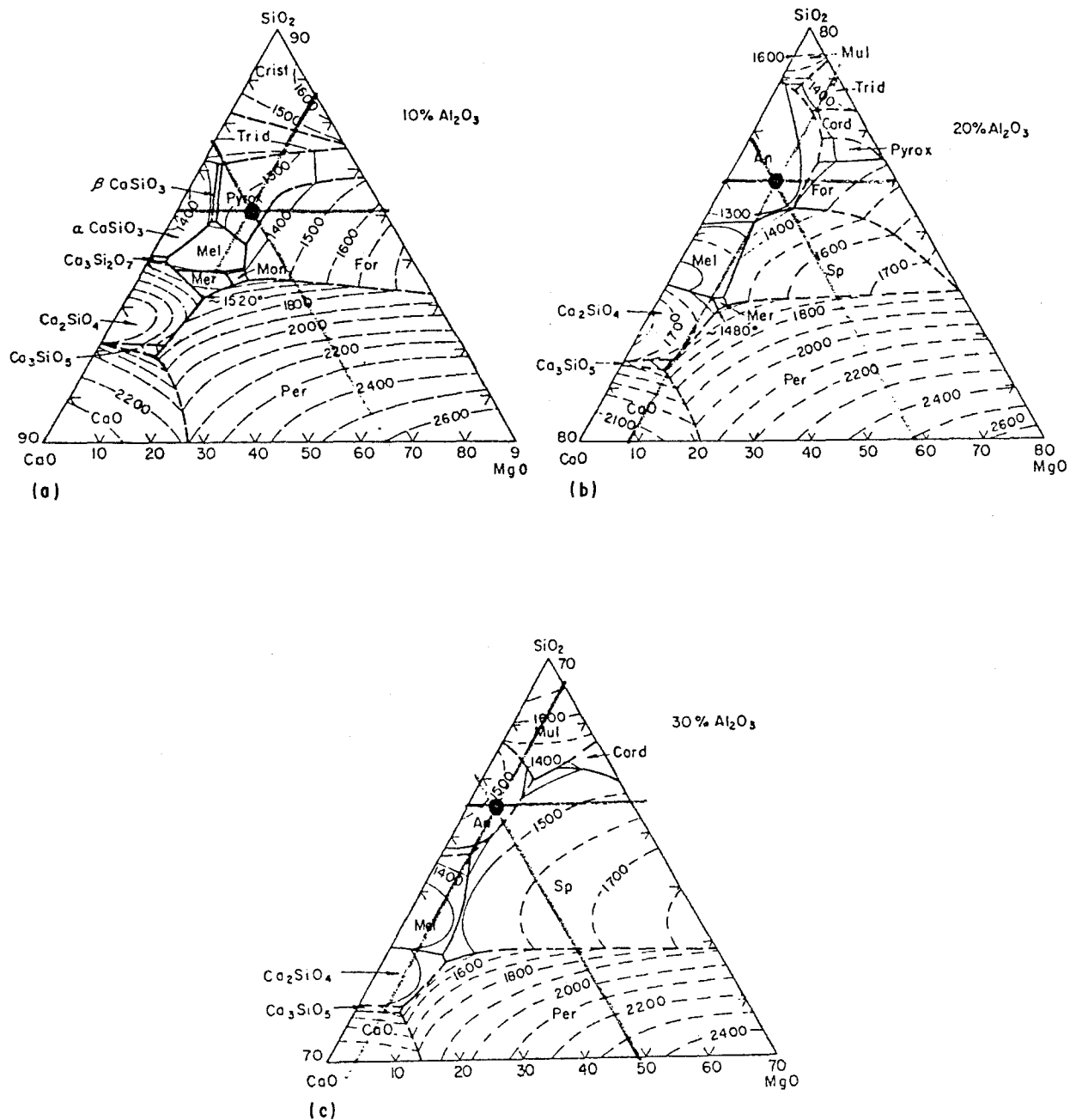


Figure 1 Phase diagrams of the system CaO–MgO–SiO<sub>2</sub> at different Al<sub>2</sub>O<sub>3</sub> contents [11]: (a) A25-D75, (b) A50-D50, (c) A75-D25.

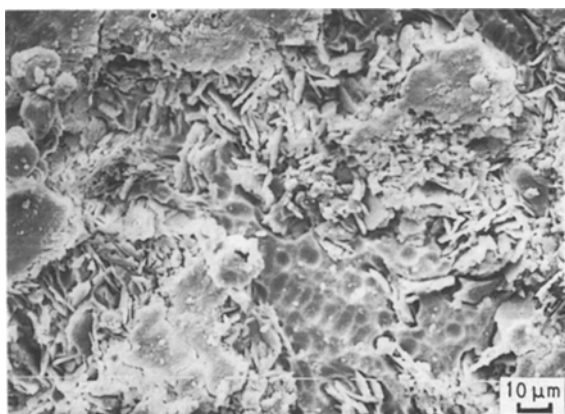


Figure 2 SEM micrograph of A75-D25 specimen just quenched in water (etched 10 min with 0.5% HF, 640×).

ensuring the absence of stresses during the ceramization process. This result is not common for glass–ceramic materials. Values for the linear expansion

coefficient from 25 to 800°C of the ceramized bodies,  $75 \times 10^{-7} \text{°C}^{-1}$  for A50-D50 and  $85 \times 10^{-7} \text{°C}^{-1}$  for A25-D75 show the trend of natural crystals:  $45 \times 10^{-7} \text{°C}^{-1}$  for pure anorthite and  $75 \times 10^{-7} \text{°C}^{-1}$  for pure diopside.

### 3.2. Microstructural and density determination

The A50-D50 and A25-D75 systems start from an amorphous phase, while the A75-D25 starts from an essentially crystalline phase. After the thermal treatment, two highly crystalline phases in different ratios, directly dependent on the glass initial composition, are present in all the samples, as shown in Fig. 6 which reports the XRD patterns of the systems in the glassy and ceramized state. The shape and position of the reflections closely agree with those assigned to anorthite (CaAl<sub>2</sub>Si<sub>2</sub>O<sub>8</sub>) and diopside (CaMgSi<sub>2</sub>O<sub>6</sub>)

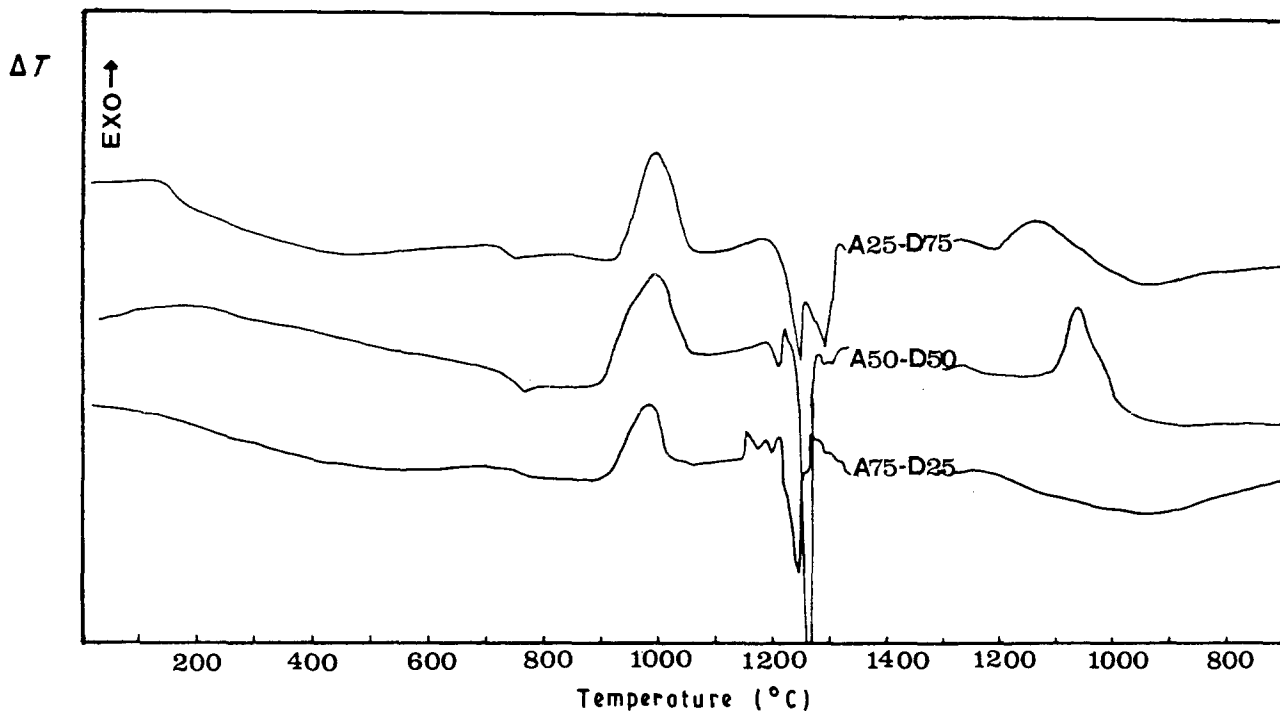


Figure 3 Heating and cooling DTA curves of the glassy compositions studied (particle size = 200  $\mu\text{m}$ ; heating and cooling rate = 10  $^{\circ}\text{C min}^{-1}$ ).

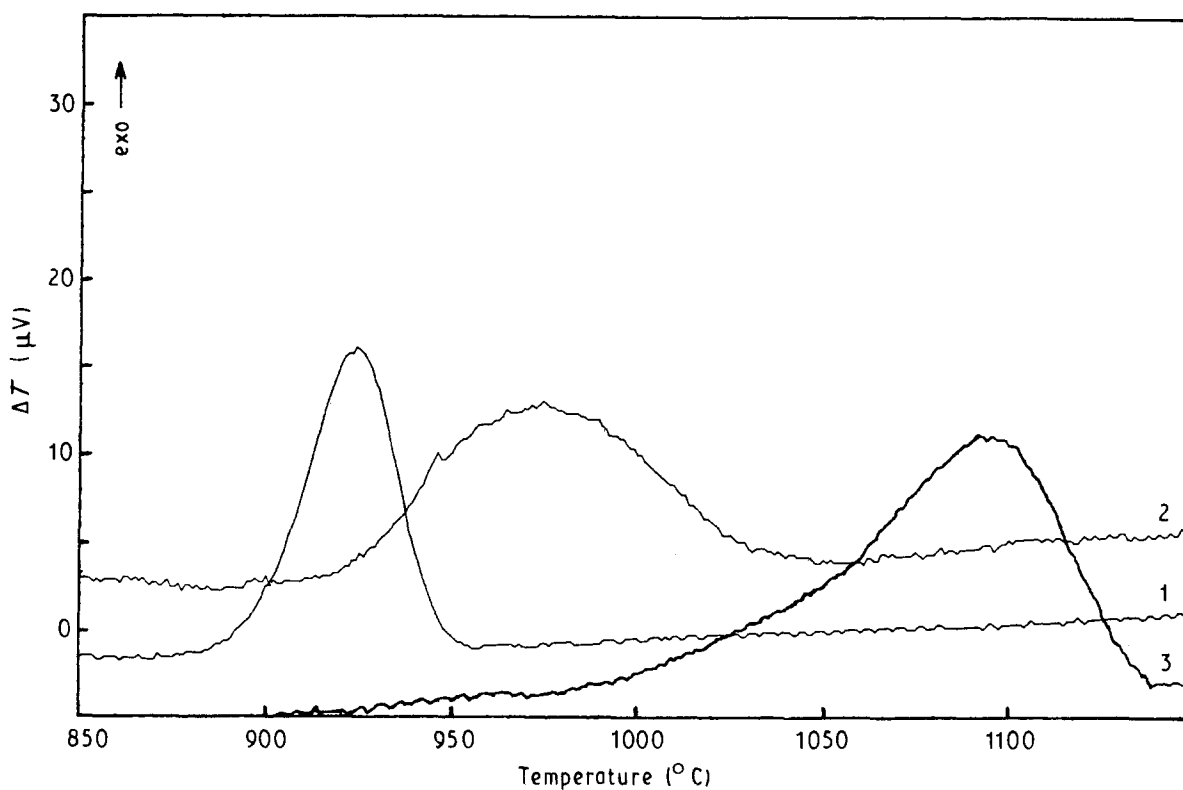


Figure 4 DTA curves at 10  $^{\circ}\text{C min}^{-1}$  of A25-D75 glass samples with different sizes: (1) < 20  $\mu\text{m}$ , (2) 200  $\mu\text{m}$ , (3) bulk.

TABLE II DTA characteristic data for glass samples with varying particle size collected at 10  $^{\circ}\text{C min}^{-1}$  heating rate

Particle size	A25-D75		A50-D50	
	$T_G$ ( $^{\circ}\text{C}$ )	$T_{\text{cryst.}}$ ( $^{\circ}\text{C}$ )	$T_G$ ( $^{\circ}\text{C}$ )	$T_{\text{cryst.}}$ ( $^{\circ}\text{C}$ )
Bulk	730	1095	740	1060
200 $\mu\text{m}$	730	975	730	1000
< 20 $\mu\text{m}$	730	920	740	910

(JCPDS File Nos 12-301 and 11-654). The peak intensities, related to the crystallinity of these two phases, are not increased by varying soak temperatures and times. This indicates that ceramization of all systems is always complete, leaving if any, undetectable traces of residual glassy phase, suggesting that the crystal phases are only controlled by the ratio  $\text{MgO}/\text{Al}_2\text{O}_3$ .

SEM micrographs (Fig. 7) performed on a section of 1 mm diameter rod from ceramized A50-D50 composition confirm the surface crystallization mechanism

and exhibit a change of volume during the devitrification. The crystals have a higher density than the parent glass, suggested by the presence of interlocking crystals with a radial distribution (Fig. 7b) and a circular cavity inside.

Fig. 8 shows that density values for crystalline materials, slightly higher than those obtained for glasses, are positioned on the straight line connecting the density values of pure anorthite and diopside crystals. The nearly perfect additivity of the density values confirms that these glass-ceramics are almost completely crystalline. The high value representing A75-D25 sample density, as it comes out of the crucible, indicates the presence of a large portion of crystallized material.

### 3.3. Kinetics of crystallization

The completeness of devitrification in the system investigated appears relevant in spite of the fact that these materials are only surface-nucleated. In order to evaluate the activation energy for the crystallization process, we have investigated the kinetic behaviour of the system with the so-called Kissinger equation below, which can be applied in those cases where crystallization starts from the glass surface and grows towards the inside of the glass matrix one-dimensionally (Fig. 7a) [13]. The simplest equation, which correlates

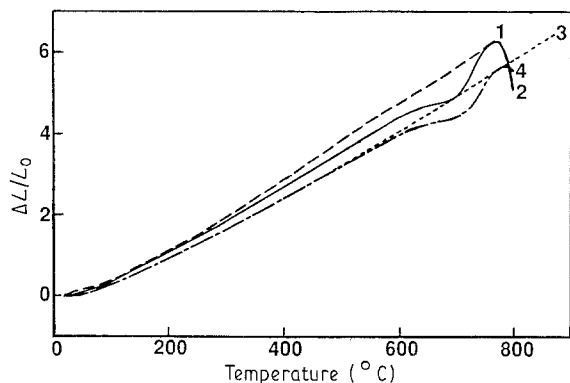
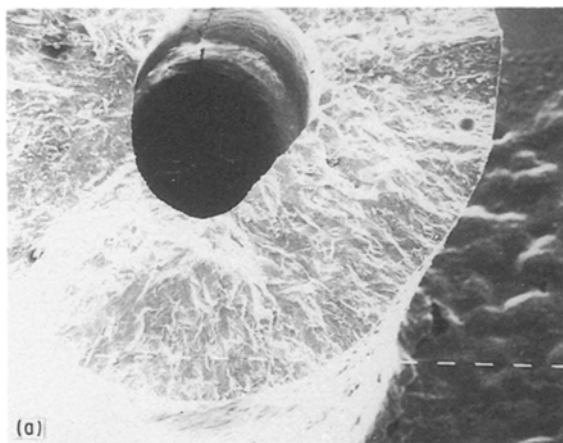


Figure 5 Dilatometric curves of 3.5 cm × 4.0 cm bars of (1) A25-D75 glass-ceramic, (2) A25-D75 non-annealed glass, (3) A50-D50 glass-ceramic, (4) A50-D50 non-annealed glass.



the peak temperature with the heating rate, is derived on the basis of the nucleation and growth equations. Assuming that the crystallization process is a first-order reaction, its expression is

$$\ln(a/T_0^2) = -(E/RT_0) + \text{const}$$

where  $a$  is the heating rate ( $\text{K min}^{-1}$ ) at which DTA curves have been recorded;  $T_0$  (K) is the maximum peak temperature of the crystallization exothermic peak, considering together anorthite and diopside formation;  $E$  is the activation energy of the global crystallization process expressed in  $\text{kcal mol}^{-1}$  if  $R$  (gas constant) is  $1.9872 \text{ cal mol}^{-1} \text{ K}^{-1}$ .

$T_0$  values for A50-D50 and A25-D75 systems have been determined by DTA analyses run at different heating rates on non-annealed glass finely ground in an agate mortar (grain size mean diameter of  $20 \mu\text{m}$ ) (Table III). In Fig. 9 the so-called Kissinger plot is reported. The activation energy values (Table IV),

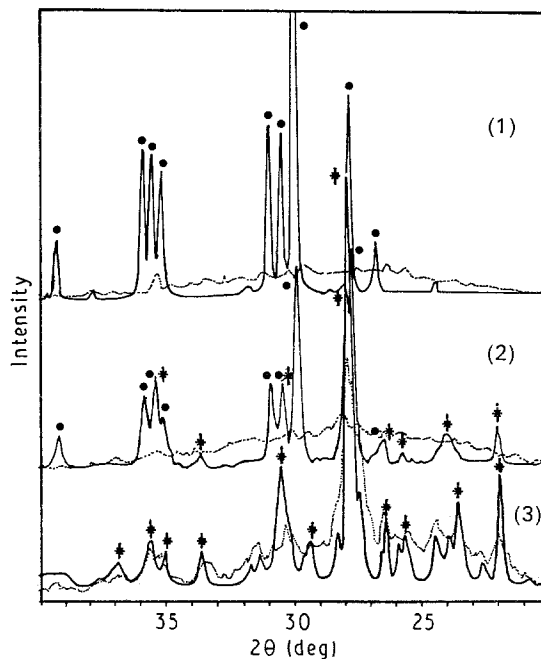


Figure 6 X-ray powder diffraction patterns of the three glass compositions in (· · ·) glassy and (—) ceramized state: (1) A25-D75, (2) A50-D50, (3) A75-D25. (● diopside; ◆ anorthite)

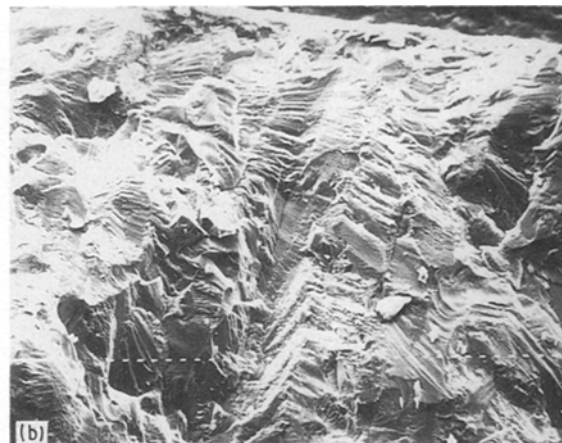


Figure 7 (a) SEM micrograph on freshly fractured A50-D50 glass-ceramic rod ( $40\times$ ); (b) a detail ( $640\times$ ).

TABLE III DTA characteristic data for glass samples with mean diameter < 20  $\mu\text{m}$  collected at different heating rates

Heating rate ( $^{\circ}\text{C min}^{-1}$ )	A25-D75		A50-D50	
	$T_G$ ( $^{\circ}\text{C}$ )	$T_{\text{cryst.}}$ ( $^{\circ}\text{C}$ )	$T_G$ ( $^{\circ}\text{C}$ )	$T_{\text{cryst.}}$ ( $^{\circ}\text{C}$ )
20	740	945	750	930
10	730	920	740	910
5	710	910	720	890

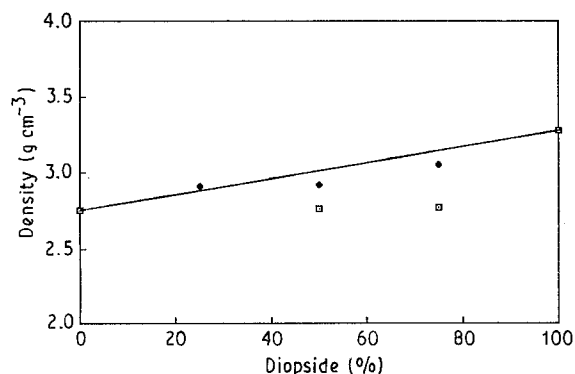


Figure 8 Sample density variations before and after the ceramization process: ( $\square$ ) glassy, ( $\blacklozenge$ ) crystallized.

calculated from the slope of the straight lines, agree with those reported in the literature for similar compositions [14].

#### 4. Conclusions

1. Only two of the possible silicates or aluminosilicates were formed.

2. Complete crystallization was obtained, even in large samples, without any addition of nucleating agents, any nucleating pre-heating treatment nor long intervals at the devitrification temperature.

3. The feldspar anorthite and the pyroxene diopside formed simultaneously from the amorphous material, leaving a glass composition such as to allow slow flow of glassy phase toward crystallization areas, thus forming spherical and irregular holes. This observation suggests that viscous flow has a lower activation energy than that for the crystallization process.

4. A parent glass and ceramized material were obtained that showed very slight differences in their physical properties.

#### Acknowledgements

We are particularly grateful to Esmalglass S.p.A., Sassuolo, Italy, for useful collaboration and support and to M.U.R.S.T. for financial support.

TABLE IV Activation energies for crystallization process derived from the so-called Kissinger equation plot for compositions A50-D50 and A25-D75 and two compositions from [14]

Composition	$E$ (kcal mol $^{-1}$ )*
A50-D50	121
A25-D75	116
Comp. 1 $^{\dagger}$	86
Comp. 2 $^{\ddagger}$	145

\* 1 cal = 4.1868 J.

$^{\dagger}$  43SiO $_2$ -18Al $_2$ O $_3$ -23CaO-0.9Na $_2$ O-0.5K $_2$ O-1.3Fe $_2$ O $_3$ .

$^{\ddagger}$  52SiO $_2$ -10Al $_2$ O $_3$ -18CaO-18MgO-5Na $_2$ O-3K $_2$ O-1.2Fe $_2$ O $_3$ .

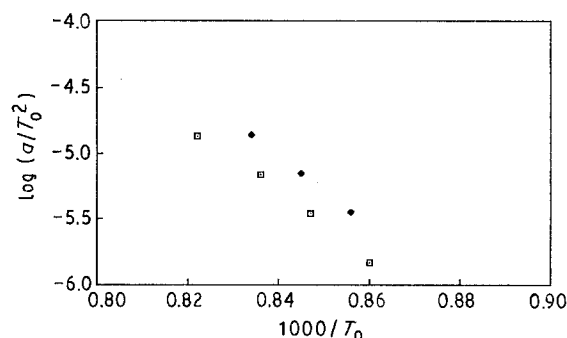


Figure 9 Plot of the so-called Kissinger equation: ( $\square$ ) A25-D75, ( $\blacklozenge$ ) A50-D50.

#### References

1. Z. STRNAD, in "Glass Science and Technology 8" (Elsevier, New York, 1986) pp. 55-76, 111, 145-150.
2. N. P. BANSAL, R. H. DOREMUS, A. J. BRUCE and C. T. MOYNIHAN, *J. Amer. Ceram. Soc.* **66** (1983) 233.
3. A. MAROTTA, A. ARONNE, P. PERNICE and F. BRANDA, *Thermochim. Acta* **140** (1989) 191.
4. S. KNICKERBOCKER, M. R. TUZZOLO and S. LAW-HORNE, *J. Amer. Ceram. Soc.* **72** (1989) 1873.
5. A. BURI, A. MAROTTA and P. GIORDANO ORSINI, *Ceramurgia* **1** (1971) 100.
6. L. NICOLINI and F. LANZI, *Ceramurgia* **5** (1975) 86.
7. A. A. OMAR, S. M. SALMAN and My. MAHMOUD, *Ceramurgia* **15** (1985) 57.
8. A. MAJUMDAR and R. K. GUPTA, *Trans. Indian Ceram. Soc.* **45** (1986) 118.
9. R. M. MARTENS, M. ROSENHAUER, H. BUTTNER and K. VON GEHLEN, *Chem. Geol.* **62** (1987) 49.
10. A. BURI, A. MAROTTA and P. GIORDANO ORSINI, *Ceramurgia* **3** (1973) 139.
11. A. MUAN and E. F. OSBORN, in "Phase Equilibria among Oxides in Steelmaking" (Addison-Wesley, Reading, MA, 1965).
12. P. W. McMILLAN, *J. Non-Cryst. Solids* **52** (1982) 67.
13. K. MATSUDA and S. SAKKA, *ibid.* **38/39** (1980) 741.
14. N. K. CHAKRABORTY, S. K. DAS, S. K. NIYOGI and R. L. THAKUR, in Proceedings of 10th International Congress on Glass, Kyoto, Japan, 9 July 1974, Vol. 14 (1974) p. 75.

Received 17 July

and accepted 30 December 1990